Available online at www.sciencedirect.com
ScienceDirect
Geochimica et Cosmochimica Acta 70 (2006) 4734–4749
Geochimica
www.elsevier.com/locate/gca

Rb–Sr and K–Ar systems of biotite in surface environments regulated by weathering processes with implications for isotopic dating and hydrological cycles of Sr isotopes

Gi Young Jeong [a,*], Chang-Sik Cheong [b], Jeongmin Kim [b]

[a] Department of Earth and Environmental Sciences, Andong National University, Andong 760-749, Republic of Korea
[b] Geochronology Team, Korea Basic Science Institute, Daejeon 305-333, Republic of Korea

Received 19 December 2005; accepted in revised form 11 July 2006

Abstract

Biotite is widely used for Rb–Sr and K–Ar isotopic dating and influences Sr isotope geochemistry of hydrological regimes. The isotopic system of biotite behaves diversely in response to surface weathering; i.e. the complete preservation of original Rb–Sr and K–Ar isotopic ages or dramatic reduction. In this study, we have explored the relation between the behavior of isotopic systems and complex weathering processes of biotites in the weathering profiles distributed on the Mesozoic granitoids in South Korea. In the lower parts of the profiles, biotite in the early stages of weathering was transformed into either oxidized biotite or hydrobiotite, with a mass release of ^{87}Sr and ^{40}Ar forced by the rapid oxidation of ferrous iron. During the transformation to oxidized biotite, ^{87}Sr and ^{40}Ar were preferentially released relative to Rb and K, respectively, via solid-state diffusion through the biotite lattice, resulting in a drastic reduction of original isotopic age. The reduction of Rb–Sr age was greater than that of K–Ar age because K was preferentially released over Rb whereas ^{87}Sr and ^{40}Ar were released proportionally to each other. However, during the transformation of biotite to hydrobiotite (i.e., to regularly interstratified biotite-vermiculite), ^{87}Sr, Rb, ^{40}Ar, and K were completely retained in the alternating biotite interlayer, and thus the original isotopic age can be preserved. In the upper parts of the profiles, where iron oxidation was almost completed, ^{87}Sr, Rb, ^{40}Ar, and K were gradually and proportionally released, with no further significant change in isotopic age during the gradual transformation of the early-formed oxidized biotite into hydrobiotite and vermiculite or during their final decomposition to kaolinite. The ratios and amounts of isotopes released from weathered biotites are dependent upon the degree of iron oxidation and the pathways of mineralogical transformation. Regional and local variations in isotopic systems affected by particular weathering processes should be considered when dating biotite or biotite-bearing rocks in weathering environments, modeling the transfer of Sr isotopes to hydrologic regimes, and tracking the provenance of sediments.

1. Introduction

Biotite is an important reservoir of Rb–Sr and K–Ar isotopes, which are useful in dating lithological units (Faure, 1986; McDougall and Harrison, 1999) and tracing the provenance of biotite-bearing sediments (Michell and Taka, 1984; Mitchell et al., 1988; Renne et al., 1990). Weathering biotite releases inorganic nutrients essential for plant growth (Scott and Amonette, 1988) and Sr isotopes useful in tracing regional and global hydrological cycles (Brass, 1976; Palmer and Edmond, 1989; Edmond, 1992; Krishnaswami et al., 1992; Richter et al., 1992; Blum et al., 1994; Blum and Erel, 1997; Bullen et al., 1997; Erel et al., 2004). Although the weathering of biotite has been widely studied in many disciplines, there still remain many uncertainties regarding isotopic systems under weathering environments, especially in mineralogical viewpoints.

Rb–Sr and K–Ar isotopic systems of biotite subjected to weathering were already investigated in the early days of their geochronological application, and diverse behaviors

* Corresponding author.
E-mail address: jearth@andong.ac.kr (G.Y. Jeong).

0016-7037/$ - see front matter © 2006 Elsevier Inc. All rights reserved.
doi:10.1016/j.gca.2006.07.012

of these isotopic systems have been reported since then. Goldich and Gast (1966) observed that weathering drastically reduced Rb–Sr ages even in the incipient stages of weathering. Clauer (1981) and Clauer et al. (1982) showed that both the K–Ar and Rb–Sr ages of weathered biotites were dramatically reduced. Mitchell et al. (1988) also reported a significant reduction of K–Ar ages in the biotites of weathered granites. On the other hand, Kulp and Engels (1963) showed in their column experiments that K–Ar and Rb–Sr ages remain unchanged after the removal of 50% of K. One sample of weathered biotite in Mitchell et al. (1988) completely retained the original K–Ar age. Zartman (1964) studied the effects of weathering on the K–Ar systems of biotite in one weathered granite, and observed no change in K–Ar age. However, there is no explanation on the diverse responses of Rb–Sr and K–Ar isotopic systems of biotite subjected to weathering from the complete preservation of original isotopic ages to dramatic reduction.

A geochemical mass balance study of a granitic watershed indicated that biotite weathering plays a critical role in the $^{87}Sr/^{86}Sr$ ratio of stream water and soil exchangeable pool because its $^{87}Sr/^{86}Sr$ ratio is significantly high and readily affected by weathering (Blum et al., 1994; Blum and Erel, 1997; Erel et al., 2004). Despite the general agreement on the important role of biotite in the geochemical and Sr isotopic compositions of water and soils, detailed mass balancing is not straightforward, for which several assumptions should be made about the weathering mechanism of biotites.

Previous isotopic studies of weathered biotite have usually overlooked the complex mineralogical and chemical changes in the course of weathering, which inevitably disturb isotopic systems. On the other hand, numerous mineralogical investigations have lacked systematic isotopic data. Biotite passes through several pathways of structural transformation to hydrobiotite (1:1 regularly interstratified biotite-vermiculite), discrete vermiculite, oxidized biotite or their mixtures (Scott and Amonette, 1988; and references therein; Jeong and Kim, 2003; and references therein; Murakami et al., 2003). It is highly likely that these diverse pathways have some connections with the diverse responses of biotite isotopic systems to weathering. To clarify this interesting issue, here we combined detailed mineralogical investigations with Rb–Sr, K–Ar, and Ar–Ar isotopic analyses of biotites systematically collected from weathering profiles well developed on Mesozoic granitoids in South Korea, and suggest a new model on the behaviors of the isotopic systems of biotite subjected to weathering. Implications for isotopic dating and hydrological cycles of Sr isotopes will be also discussed.

2. Samples

Granitoid rocks constitute major lithological units in South Korea that intruded over a wide geological time scale ranging from the Precambrian to early Tertiary (Fig. 1). Of these, the Jurassic and Cretaceous granitoids

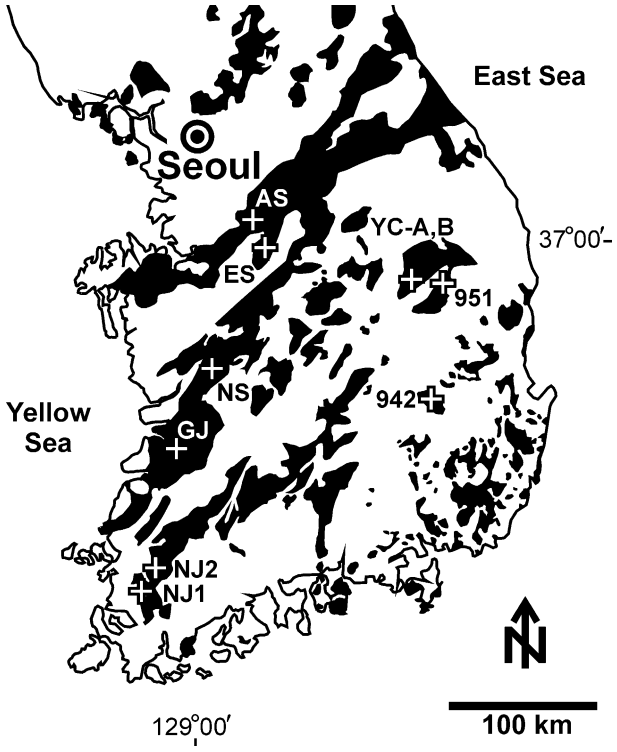

Fig. 1. Distribution of Mesozoic granitoids in South Korea and locations of the weathering profiles (cross) investigated in this study.

are the most widespread plutons. The granitic rocks have more homogeneous fabrics, mineralogy, and chemistry than other biotite-bearing rocks, so that their weathering profiles are good candidates for a systematic study of biotite weathering. Biotite is usually a primary magmatic mineral of granitoids. It is either pristine or altered in varying degrees to chlorite, zoisite, epidote, and titanite.

The study areas are located in the middle latitudes of the northern hemisphere, and belong to the humid temperate climate zone with four distinct seasons. The mean annual air temperature of the study areas ranges from 10 to 16 °C while the mean annual precipitation ranges from 1000 to 1400 mm. About 50% of the annual precipitation falls between June and August. Under humid temperate climatic conditions, weathering profiles are well developed in the granitoid outcrops. Ten weathering profiles (942, 951, AS, ES, GJ, NJ1, NJ2, NS, YC-A, and YC-B) were selected for this study (Fig. 1). A complete transect from fresh rock to thick saprolite and reddish brown soil is exposed by recent road cutting and stone quarrying (profiles 942, 951, AS, NJ2, NS, and YC-A), but in some sites, the fresh bedrock underlying the saprolite is not exposed in the very deeply weathered outcrops (profiles ES, GJ, NJ1, and YC-B). Samples weighing 2–3 kg were systematically collected throughout the weathered profile from fresh rock to the uppermost soil at intervals of 1–2 m, on the basis of changes in biotite color and the mechanical strength of the samples. In the Yecheon area, profile YC-A is separated from profile YC-B by about 100 m. Fresh bedrock is exposed in the lowermost part of profile

YC-A, but not in profile YC-B. Jeong and Kim (2003) showed that profile YC-B is the more weathered equivalent of profile YC-A. Granitoids underlying all the weathering profiles except the 942 site are Jurassic in intrusion ages (197–158 Ma; Sagong et al., 2005). The 942 profile is developed on Cretaceous granite (75 Ma; Cheong et al., 1998).

3. Methods

Biotite grains 0.15–0.35 mm in diameter were separated by wet sieving, magnetic separation, and hand sorting under a stereomicroscope. The biotite concentrates were ground under acetone to prevent iron oxidation, and X-ray diffraction (XRD) patterns were obtained from the oriented samples after Mg saturation and ethylene glycol saturation using a Rigaku D/MAX2200 instrument equipped with a Cu target operating at 40 kV/30 mA. The iron oxidation states of fresh biotites and hydrobiotites in profile 942 were determined for one hundred milligrams of concentrate mixed with sugar and ground under acetone by Mössbauer spectroscopy at the Department of Physics, Pukyong National University, South Korea. Their chemical compositions were analyzed for polished thin sections using a Cameca SX51 electron probe microanalyzer (EPMA) at Korea Basic Science Institute (KBSI), Daejeon, South Korea.

The Rb–Sr isotopic compositions of biotites, plagioclases, and whole rock powders were analyzed for profiles YC-A, YC-B, AS, and 942. Isotopic analyses were performed at KBSI. Several 10 mg of separated minerals and whole-rock powders were mixed with highly enriched ^{84}Sr and ^{87}Rb spikes and then dissolved with a mixed acid ($HF/HClO_4 = 10:1$) in Teflon vessels. Rb and Sr fractions were separated by conventional cation column chemistry (Dowex AG50W-X8, H^+ form) in HCl medium. Isotopic ratios were measured using a VG54-30 thermal ionization mass spectrometer equipped with nine Faraday cups. Instrumental fractionation was normalized to $^{86}Sr/^{88}Sr = 0.1194$ and the measured $^{87}Sr/^{86}Sr$ ratio was further corrected for the contributions of the added spikes. Replicate analysis of NBS 987 gave a mean $^{87}Sr/^{86}Sr$ of 0.710246 ± 0.000004 ($n = 14$, 2σ SE). Total procedural blank levels were around 30 pg for Rb and 120 pg for Sr. Isochron parameters were calculated according to Ludwig (2001) and errors in reported ages are given at 95% confidence level.

The radiogenic ^{40}Ar content of both fresh and weathered biotites was measured for all the pofiles using a VG5400 static vacuum mass spectrometer, and their K contents were analyzed using a Unicam 989 atomic absorption spectrometer at KBSI. Standard air is used to obtain the discrimination factor between Ar isotopes.

For ^{40}Ar–^{39}Ar dating, biotite grains were wrapped with the pure (<99.5%) aluminum foil and set into a sample bucket. Flux monitoring minerals (Fisher Canyon sanidine, Renne et al., 1998) and salt (CaF_2 and K_2SO_4) were also prepared to correct interfering isotopes during irradiation. The sample bucket was placed into an irradiation target made from pure aluminum and irradiated for four days in the IP11 position of the "Hanaro" reactor in the Korea Atomic Energy Research Institute. After irradiation, the samples and flux monitoring materials were placed in the glass sample chamber of the gas preparation system at KBSI. Samples were heated from 500 to 1450 °C with increment intervals of 40–60 °C. The extracted gas was purified and analyzed using the VG5400 mass spectrometer to measure Ar isotopes by the peak-jumping method.

4. Results

4.1. Pathways of biotite weathering

In the investigated weathering profiles, fresh biotite was transformed into oxidized biotite, hydrobiotite, or hydrobiotite via oxidized biotite (Figs. 2–4). Although a small

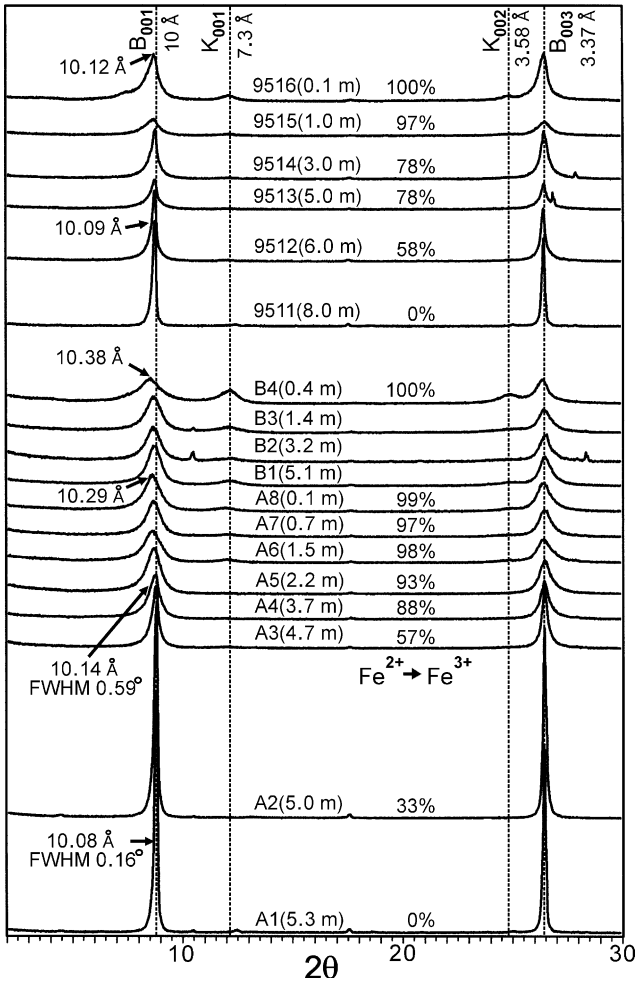

Fig. 2. X-ray diffraction patterns of the oriented mounts of the biotites from the profiles 951 (samples 9511–9516), YC-A (samples A1–A8), and YC-B (samples B1–B4). Oxidized biotite is the major weathering product of fresh biotite (samples 9511 and A1). Depth in meter below ground surface is indicated in brackets. Percent indicates the oxidation degree of ferrous iron of biotite. FWHM, full width at half maximum of the XRD peak; B, biotite; K, kaolinite.

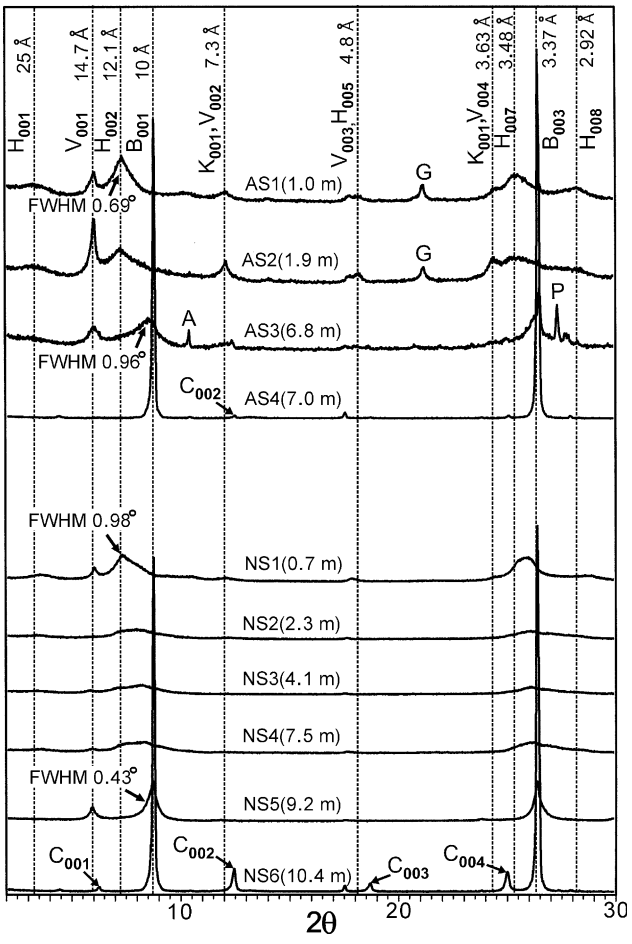

Fig. 3. X-ray diffraction patterns of the oriented mounts of the biotites from the profiles AS (samples AS1–AS4) and NS (samples NS1–NS6). Oxidized biotite (samples AS3 and NS5) developed from fresh biotite was transformed into hydrobiotite (samples AS1, AS2, and NS1). Depth in meter below ground surface is indicated in brackets. FWHM, full width at half maximum of the XRD peak; A, amphibole; B, biotite; C, chlorite; G, goethite; H, hydrobiotite; K, kaolinite; P, plagioclase; V, vermiculite.

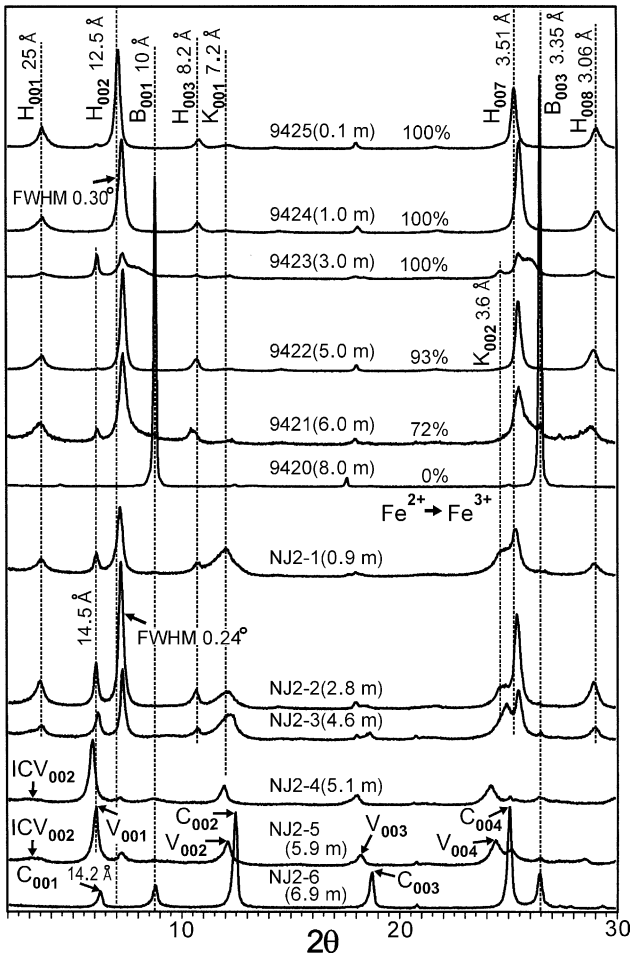

Fig. 4. X-ray diffraction patterns of the oriented mounts of the biotites from the profiles 942 (samples 9421–9425) and NJ2 (samples NJ2-1–NJ2-6). Hydrobiotite is the major weathering product of fresh biotite (sample 9420) throughout the profile 942, but in the upper three samples (NJ2-1, -2, and -3) in the profile NJ2. Depth in meter below ground surface is indicated in brackets. Percent indicates the oxidation degree of ferrous iron of biotite. FWHM, full width at half maximum of the XRD peak; B, biotite; C, chlorite; H, hydrobiotite; ICV, interstratified chlorite-vermiculite; K, kaolinite; V, vermiculite.

amount of vermiculite is associated with weathered biotites, it is not a major weathering product, at least in our samples. In the granitic bedrocks, partial chloritization of biotite before weathering was common and significant in some profiles (e.g., NJ2). In the very early stages of weathering, chlorite admixed with biotite tends to be transformed into vermiculite or interstratified chlorite-vermiculite (ICV), with the enhancement of relative intensity of the XRD peak at 14–15 Å. Thus, both the vermiculite and the ICV derived from chlorite can be misidentified as having transformed from biotite, requiring a careful interpretation of the mineralogical nature of the weathered biotite.

4.1.1. Transformation to oxidized biotite

Oxidized biotite was a major transformation product of biotite in eight weathering profiles (951, ES, GJ, NJ1, YC-A, and YC-B) (Fig. 2). Oxidized biotite is characterized by a 10 Å peak in the XRD pattern and the almost complete oxidation of iron. In profile YC-A, 88% of Fe^{2+} was oxidized in sample A4 (3.7 m depth), and then the proportion increased gradually to 99% in sample A8 (0.1 m depth) (Fig. 2). 100% of Fe^{2+} was oxidized in the sample B4 of profile YC-B (Fig. 2). A basal spacing of 10 Å is maintained well throughout the profile. Lattice imaging by transmission electron microscopy also showed that oxidized biotite consists mostly of 10Å layers (Jeong and Kim, 2003). The period of active iron oxidation from A1 to A4 coincides with a dramatic decrease in the peak height of d_{001}, a very slight increase in d_{001}-spacing of only about 0.06 Å, and an increase in the full width at half maximum (FWHM) from 0.16° to 0.59° in 2θ (Fig. 2). Although the oxidized biotite is a major component of the weathered biotite, vermiculite is commonly associated with the oxidized biotite. According to XRD pattern simulations using the NEWMOD program (Reynolds, 1985), a slight

increase in d_{001} spacing and a large increase in $FWHM_{001}$ indicate the presence of a small amount of vermiculite randomly interstratified with biotite (less than 10%). The structural formula of the oxidized biotite in profile YC-A, derived by Jeong and Kim (2003), is given in Table 1. They showed that the structural and chemical modifications in the formation of oxidized biotite were a b_o-dimension decrease and the non-stoichiometric removal of interlayer K and octahedral Mg and Fe to compensate for the charge imbalance induced by iron oxidation.

In profile 951, iron oxidation also occured in the lower part of the weathering profile. 78% of Fe^{2+} was rapidly oxidized up to sample 9513 (5 m depth), and the proportion gradually approached 100% in sample 9516 (0.1 m depth). In profiles 951, ES, GJ, NJ1, YC-A, and YC-B, oxidized biotite persisted throughout the profile with very slight but gradual vermiculitization and decomposition into kaolinite.

In profiles AS and NS, biotite was rapidly transformed to oxidized biotite (samples AS3 and NS5) in the early stages of weathering, and then transformed gradually into hydrobiotite (Fig. 3). The major pathways of structural transformation of biotite in the profiles YC and AS are graphically summarized in Fig. 5.

Oxidized biotite in the weathering profiles has generally been overlooked in the study of biotite weathering and is often not distinguished from fresh biotite. However, the oxidized biotite should be considered a common type of transformation in the weathering of biotite because its chemistry and detailed structure are different from those of fresh biotite and it is considerably stable in the weathering profile. Oxidized biotite has been widely reported in the deeply weathered soil-saprolite profiles developed on granitic terranes under humid tropical (Murphy et al., 1998), mediterranean (Fordham, 1990), and temperate climates (Harris et al., 1985).

Table 1
Formulas of fresh biotites, oxidized biotite, and hydrobiotite derived from the electron microprobe data

	Fresh biotite (profile YC-A)	Oxidized biotite (profile YC-A)	Fresh biotite (profile 942)	Hydrobiotite (profile 942)
Si	5.50	5.51	5.53	5.53
Al(IV)	2.50	2.49	2.30	2.30
Fe^{3+}(IV)	0.00	0.00	0.17	0.17
Sum	8.00	8.00	8.00	8.00
Al(VI)	0.40	0.32	0.00	0.00
Fe^{2+}	2.08	0.00	1.81	0.00
Fe^{3+}(VI)	0.50	2.24	0.40	1.77
Fe(total)	2.58	2.24	2.21	1.77
Mg	2.17	1.98	2.72	2.46
Ti	0.33	0.30	0.57	0.54
Mn	0.04	0.03	0.03	0.02
Sum	5.52	4.87	5.52	4.78
Octahedral occupancy (%)	92	81	92	80
Octahedral charge	12.6	12.9	12.6	12
Ca	0.01	0.04	0.00	0.05
Na	0.02	0.01	0.03	0.05
K	1.87	1.51	1.85	1.01
$Al(OH)^{2+}$	—	—	0.00	0.45
Interlayer charge	1.91	1.60	1.89	2.07

4.1.2. Transformation to hydrobiotite

In profile 942, biotite was transformed directly into hydrobiotite by the hydration and expansion of alternating interlayers in the early stages of weathering (Fig. 4). Mössbauer spectroscopy showed that 72% of the original Fe^{2+} was oxidized in sample 9421, and 93% in sample 9422. Before iron oxidation was completed, the biotite was almost completely transformed into hydrobiotite in sample 9421, and this persisted throughout the profile, with only partial decomposition to kaolinite in the uppermost sample 9425. XRD pattern simulation showed that the biotite (B):vermiculite (V) ratios of the hydrobiotites in the profile 942 were $B_{55}V_{45}$ (samples 9421, 9422, and 9424) and $B_{46}V_{54}$(9425). However, sample 9423 was a mixture of $B_{82}V_{18}$, $B_{58}V_{42}$, and discrete vermiculite in a ratio of 56:37:7.

The structural formula for Ca-saturated hydrobiotite in sample 9422 was derived from electron microprobe data according to the method of Jeong and Kim (2003). Hydroxy-Al cations are the major ones occupying the interlayer of vermiculite (Table 1). Hydroxy-Al-interlayered vermiculite is common in acidic weathering environments, and the hydroxy-Al cations are hard to be exchanged by other cations (Banhisel and Bertsch, 1989 and references therein). The K content per formula decreased from 1.85 in fresh biotite to 1.01 in hydrobiotite. The layer ratio based on K content is $B_{55}V_{45}$ which is consistent with that obtained from XRD pattern simulations. The pathway of structural transformation of biotite in the profile 942 is also summarized in Fig. 5.

In the profile NJ2, the biotite in fresh rock (sample NJ6) was significantly chloritized as shown in the XRD pattern (Fig. 4) and by thin-section petrography. Weathered biotites in the lower part of the profile (samples NJ4 and NJ5) consist predominantly of vermiculite with minor ICV and hydrobiotite. The vermiculite and ICV must have been transformed from chlorite in the parent rock. However, weathered biotites in the upper part of the profile (samples NJ2-1, -2, and -3) are dominated by hydrobiotite. FWHMs of the d_{002} diffraction line of hydrobiotite (0.20°–0.28°) are similar to those of the hydrobiotite in profile 942 (0.25°–0.34°). The layer ratio is about $B_{55}V_{45}$ according to XRD pattern simulations. We think that the hydrobiotite was transformed from fresh biotite that had undergone less chloritization before weathering at that position.

In profiles AS and NS, hydrobiotite gradually developed from previously oxidized biotite, which had been transformed from fresh biotite in the early stages of weathering, with formation of minor kaolinite in the upper part of the profile (Fig. 3). The d_{002} lines of hydrobiotite in profiles AS

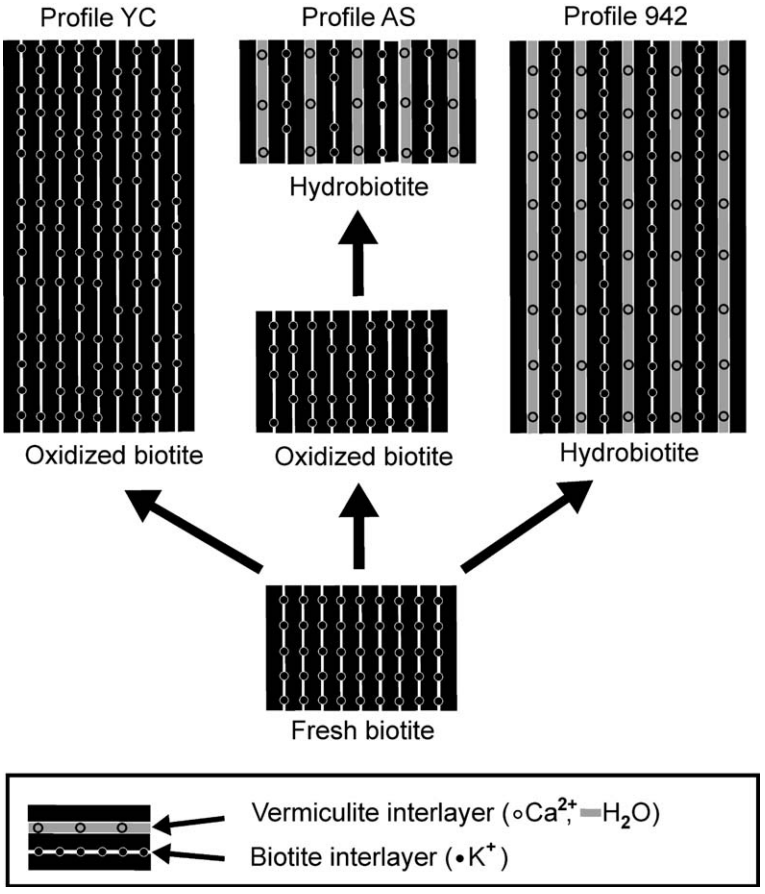

Fig. 5. Three types of pathways of structural transformation of biotite in the weathering profiles.

and NS are much broader and lower in intensity than those of hydrobiotite in profiles 942 and NJ2, and their FWHMs (0.69°–0.98°) are similar to those of oxidized biotites (AS3 0.96°, NS5 0.43°, and AS4 0.59°).

4.2. Rb–Sr and K–Ar isotopic systems of weathered biotites

4.2.1. Rb–Sr system

The Rb–Sr isotopic data of fresh and weathered biotites are given in Table 2. Because profile YC-B is the more weathered equivalent of profile YC-A, samples from the profile YC-B are arranged after those from the profile YC-A in Table 2. In profile YC, the Sr content increases abruptly from 8.51 ppm (A1) to 45.9 ppm (A2) and then gradually increases to 156 ppm (B3). Conversely, the Rb content decreases slightly by only 5% from 486 ppm in fresh biotite (A1) to 462 ppm in weathered biotite (A4) that is mostly oxidized biotite with minor vermiculite. The $^{87}Rb/^{86}Sr$ and $^{87}Sr/^{86}Sr$ ratios of fresh biotite are remarkably higher than those of fresh whole rock and plagioclase. The apparent Rb–Sr ages of weathered biotites in profile YC decrease systematically with the advance of weathering (Table 2). The decrease in age is great in the period of active iron oxidation between A1 and A4 to form oxidized biotite, but thereafter the age decreases gradually. The Rb–Sr isotopic data are plotted on the fresh whole rock–fresh biotite (A1) isochron diagram. Data of plagioclase are similar to those of whole rock, being plotted almost at the same position. All the data of weathered biotites cluster near whole rock (or plagioclase) point (Fig. 6). Magnified view of the cluster shows that data for samples in the early stages of weathering (A2–A4) deviate more and more from the isochron with advancing weathering, whereas in the later stages beyond A4, data fall close to a straight line toward the whole rock (or plagioclase) point (Fig. 6).

In profile 942, the Rb content decreases abruptly from 607 ppm (sample 9420) to 410 ppm (9421) and then decreases gradually. The Rb content of sample 9423 is higher than those of neighbouring samples. The Sr content increases from 9.45 ppm (9420) to 31.6 ppm (9421) and then gradually decreases. The $^{87}Rb/^{86}Sr$ and $^{87}Sr/^{86}Sr$ ratios of fresh biotite are enormously higher than those of fresh whole rock and plagioclase. Data except the sample 9423 are plotted on the fresh whole-rock – fresh biotite (9420) isochron (Fig. 6), giving nearly the same age. Hydrobiotites in profile 942 preserve the original age of the fresh biotite except in sample 9423. It is notable that data of hydrobiotites in the lower part of the profile (9421 and 9422) fall close to whole rock point, whereas those in the upper part of the profile (9424 and 9425) approach fresh biotite point.

Table 2
Rb–Sr isotopic data of whole rock, plagioclase and biotite from the weathering profiles YC-A, YC-B, AS, and 942 in South Korea

Sample[a]	Rb (ppm)	Sr (ppm)	$^{87}Rb/^{86}Sr$[b]	$^{87}Sr/^{86}Sr$	2s SE	Age (Ma)[c]	^{87}Sr (ppm)[d]	Retention %		
								^{87}Sr%	Rb%	Age
$B4_{WB}$	276	88.5	9.029	0.721745	0.000014	38.9 ± 0.3	0.11	12	57	24
$B3_{WB}$	303	156	5.618	0.719891	0.000014	39.3 ± 0.3	0.11	12	62	24
$B2_{WB}$	399	123	9.396	0.721525	0.000013	35.5 ± 0.2	0.14	16	82	22
$B1_{WB}$	369	115	9.276	0.722075	0.000013	40.4 ± 0.3	0.15	17	76	25
$A8_{WB}$	402	92.0	12.66	0.727767	0.000014	61.7 ± 0.3	0.26	30	83	38
$A7_{WB}$	466	106	12.74	0.725570	0.000013	48.7 ± 0.3	0.24	27	96	30
$A6_{WB}$	447	92.5	14.00	0.728641	0.000013	60.3 ± 0.3	0.29	32	92	37
$A5_{WB}$	425	85.9	14.33	0.727623	0.000013	53.6 ± 0.3	0.24	27	87	33
$A4_{WB}$	462	71.5	18.75	0.732119	0.000011	55.2 ± 0.3	0.29	33	95	34
$A3_{WB}$	450	54.5	23.99	0.750560	0.000021	98.5 ± 0.5	0.50	56	93	61
$A2_{WB}$	448	45.9	28.45	0.771802	0.000024	136.5 ± 0.7	0.68	77	92	84
$A1_{FB}$	486	8.51	171.7	1.112340	0.000024	162.2 ± 0.8	0.89	100	100	100
$B2_{WR}$	87.6	408	0.6213	0.717105	0.000011					
$A6_{WR}$	97.2	437	0.6443	0.717206	0.000010					
$A1_{FR}$	109	440	0.7184	0.717990	0.000010					
$A1_{P}$	95.1	645	0.4272	0.717353	0.000013					
$AS1_{WB}$	694	24.6	81.81	0.750016	0.000012	30.9 ± 0.2	0.11	17	82	20
$AS2_{WB}$	372	46.0	23.41	0.723886	0.000013	29.4 ± 0.2	0.06	9	44	19
$AS3_{WB}$	830	20.0	121.1	0.777610	0.000012	37.6 ± 0.2	0.16	24	98	24
$AS4_{FB}$	844	2.62	1166	3.273445	0.000032	154.5 ± 0.8	0.67	100	100	100
$AS1_{WR}$	172	315	1.583	0.714760	0.000013					
$AS4_{FR}$	152	443	0.9912	0.713556	0.000013					
9425_{WB}	220	4.20	153.8	0.862926	0.000032	71.4 ± 0.4	0.29	36	36	98
9424_{WB}	279	4.64	177.0	0.885185	0.000023	70.9 ± 0.4	0.37	45	46	98
9423_{WB}	406	14.6	80.84	0.750571	0.000016	36.9 ± 0.2	0.29	35	67	51
9422_{WB}	305	21.7	40.81	0.749674	0.000016	73.5 ± 0.4	0.42	51	50	101
9421_{WB}	410	31.6	37.63	0.743706	0.000017	68.6 ± 0.4	0.52	64	67	95
9420_{FB}	607	9.45	189.2	0.901874	0.000018	72.5 ± 0.4	0.82	100	100	100
9424_{WR}	101	88.2	3.318	0.710207	0.000008					
9422_{WR}	116	149	2.257	0.709391	0.000011					
9420_{FR}	119	226	1.516	0.708515	0.000011					
9420_{P}	12.7	552	0.0668	0.706897	0.000011					

[a] Sample types: WB, weathered biotite; FB, fresh biotite; WR, weathered whole rock; FR, fresh whole rock; P, plagioclase.
[b] Reproducibility was below 0.5%.
[c] Whole rock-biotite apparent ages.
[d] ^{87}Sr content in the biotite interlayer of the weathered biotite calculated according to the method discussed in the text. Since $^{87}Sr/^{86}Sr$ ratio of plagioclase was not measured in the profile AS, that of whole rock was used for calculation.

In profile AS, the Sr content increases abruptly from 2.62 ppm in fresh biotite (AS4) to 20.0 ppm in weathered biotite (AS3) that is mostly oxidized biotite with minor vermiculite, but the Rb content only slightly decreases during the transformation of fresh biotite to oxidized biotite, similar to the variation from sample A1 to sample A4 in profile YC. Data point of sample AS3 significantly deviates from the fresh whole rock – fresh biotite (AS4) isochron. During the transformation of oxidized biotite (AS3) to hydrobiotite (AS1 and AS2), however, data are plotted on the straight line toward the whole-rock point. The apparent Rb–Sr age decreases greatly during the transformation of fresh biotite (A4) to oxidized biotite (AS3), and thereafter shows little change during the development of hydrobiotite (AS1 and AS2).

4.2.2. K–Ar system

In accordance with the Rb–Sr system, the apparent K–Ar age of the weathered biotite decreased during the formation of oxidized biotite in the early stage of weathering. In profile YC, the K–Ar age decreases dramatically from samples A1 to A4, but then decreases very gently in the later stages (Table 3). In profile 951, the K–Ar ages decrease to 69% of the original age in sample 9512, and then decrease rather gradually. In profiles ES, GJ, and NJ3, the K–Ar ages of the weathered biotite are much younger than the ages of host Jurassic bedrocks. In profiles NS and AS, the K–Ar ages decrease greatly during the early formation of oxidized biotite, but change little during the later development of hydrobiotite from oxidized biotite.

The data for weathered biotites in profiles YC, 951, NS, AS, ES, GJ, and NJ3 are plotted on a K versus ^{40}Ar diagram (Fig. 7a). Most of the data for the weathered biotites deviate from the reference lines connecting fresh biotite to the origin. Data plot more and more away from the reference lines connecting fresh biotites to the origin in the early stages of weathering, and then, plot along straight lines connecting the oxidized biotites to the origin in the later stages.

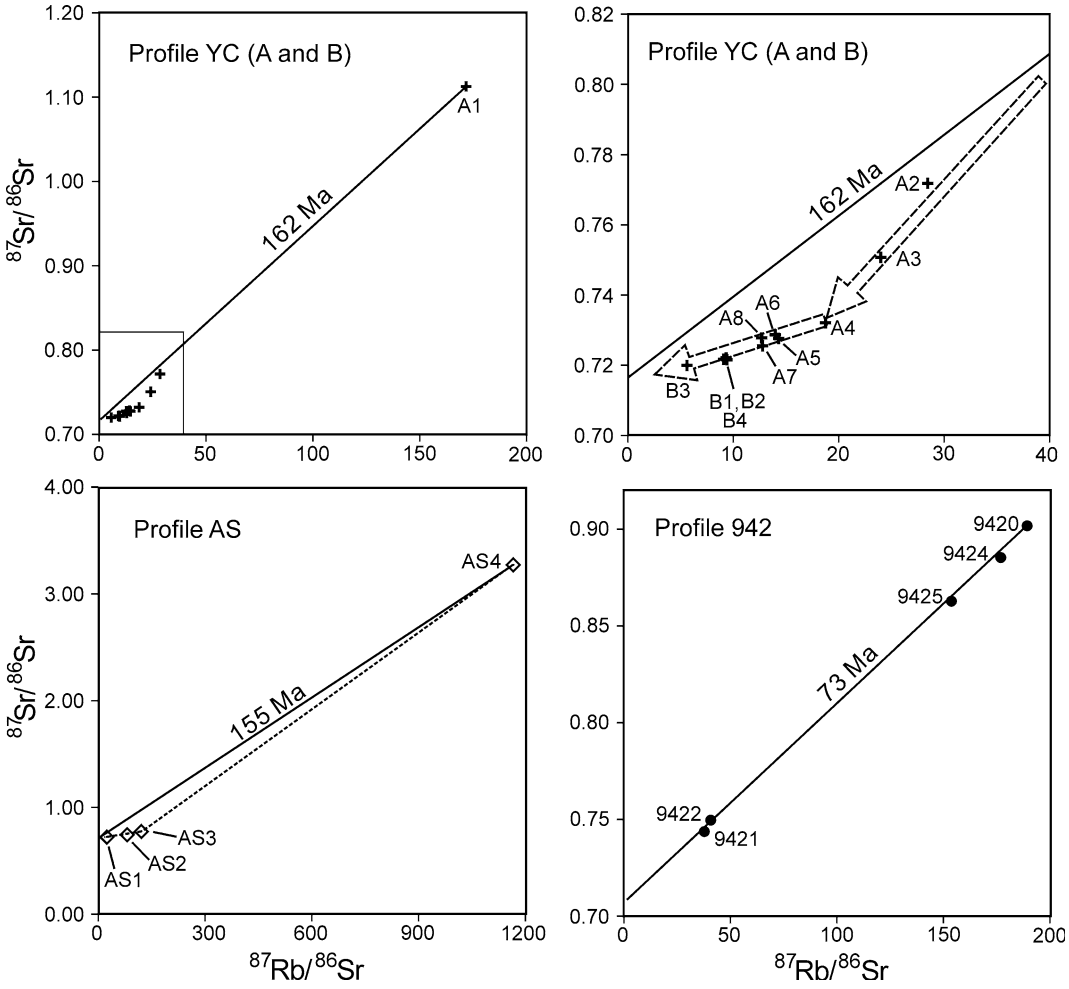

Fig. 6. Rb–Sr isotope data of the fresh and weathered biotites from four profiles (YC-A, YC-B, AS, and 942) plotted on Rb–Sr isochron diagrams. Isochron (solid lines) was calculated from data of fresh biotite and fresh whole rock. Data of profiles YC-A and -B are plotted on the same isochron diagram (see text). Dashed arrows and lines in the diagrams of profiles YC (A and B) and AS indicate that the evolution of Rb–Sr isotopic systems consists of early and later stages.

In profile 942, hydrobiotites maintain their original ages very well following the trend of the Rb–Sr system, except in sample 9423, and plot onto the reference line connecting fresh biotite to the origin (Fig. 7b). In profile NJ2, data of hydrobiotites in the upper part of the profile (samples NJ2-1, -2, and -3) are plotted on the reference line of 166 Ma which represents the cooling ages of Jurassic granitoids (Sagong et al., 2005).

^{40}Ar–^{39}Ar data were obtained from fresh biotites and their weathered counterparts in profiles YC-A (Fig. 8) and 942 (Fig. 9). In profile YC-A, the age spectrum for fresh biotite (A1) defines a plateau age of 157.3 ± 1.4 Ma, which is nearly consistent with the Rb–Sr age (162.2 ± 0.8 Ma) and the conventional K–Ar age (164.7 ± 3.2 Ma). However, the plateau is not defined in the age spectra of the weathered biotites (A4 and A7). The apparent ages increase gradually toward the high-temperature degassing steps. Total gas ages of samples A4 and A7 are 74.4 ± 2.5 Ma and 98.7 ± 2.4 Ma, respectively. The total gas age of A4 quite well accords with the conventional K–Ar age (75.5 ± 1.5 Ma), while that of A7 is slightly higher than the conventional K–Ar age (81.6 ± 1.6 Ma). In profile 942, fresh biotite (sample 9420) defines a plateau age of 74.7 ± 3.7 Ma, which is consistent with the Rb–Sr age (72.5 ± 0.4 Ma) and the conventional K–Ar age (70.2 ± 1.4 Ma). The plateau is still preserved in the age spectrum of hydrobiotite (9422), but the plateau age (284.1 ± 9.1 Ma) is four times greater than the age of fresh biotite.

5. Discussion

5.1. Origin of the diverse responses of Rb–Sr and K–Ar isotopic systems

5.1.1. Oxidized biotite

The weathered biotites in the profile YC consist of oxidized biotite with minor vermiculite layers. The abrupt increase in Sr content from sample A1 to sample A2 (Table 2) indicates the addition of Sr from an ambient weathering solution into the interlayer of vermiculite, because Sr, a large divalent cation, cannot invade the interlayer of

Table 3
K–Ar isotopic data of the fresh and weathered biotites from the weathering profiles 951, YC-A, YC-B, ES, GJ, NJ, NS, AS, 942, and NJ in South Korea

Sample[a]	K (wt%)	$^{40}Ar^{b}$ (10^{-8} ccSTP/g)	^{36}Ar (10^{-10} ccSTP/g)	Age (Ma)	Air (%)	$^{40}Ar^{b}/K$ atom ratio ($\times10^{-7}$)	Retention %		
							K	$^{40}Ar^{b}$	Age
9516_{WB}	5.17	1072.7	277.6	52.6 ± 1.1	43.3	3.6	78	21	28
9515_{WB}	5.54	1654.5	230.6	75.3 ± 1.6	29.2	5.2	84	32	40
9514wb	6.21	2434.0	195.3	98.3 ± 1.9	19.2	6.8	94	47	52
9513_{WB}	5.90	2920.1	254.6	123.2 ± 2.4	20.5	8.6	89	57	65
9512_{WB}	6.10	3208.1	135.0	130.7 ± 2.5	11.1	9.2	92	62	69
9511_{FB}	6.63	5137.4	185.9	189.3 ± 3.6	9.7	13.5	100	100	100
$B4_{WB}$	3.32	835.3	193.0	63.6 ± 1.3	40.6	4.4	43	16	39
$B3_{WB}$	4.82	916.7	413.1	48.3 ± 1.1	57.1	3.3	63	18	29
$B2_{WB}$	5.16	1044.0	326.5	51.4 ± 1.0	48.0	3.5	67	20	31
$B1_{WB}$	5.18	1164.9	365.0	57.0 ± 1.2	48.1	3.9	68	23	35
$A8_{WB}$	5.01	1534.8	223.2	78.7 ± 1.8	30.1	5.3	65	30	48
$A7_{WB}$	5.26	1705.2	222.1	81.6 ± 1.6	27.8	5.7	69	33	50
$A6_{WB}$	5.76	1732.6	268.8	75.8 ± 1.5	31.4	5.2	75	34	46
$A5_{WB}$	5.53	1384.4	268.9	63.4 ± 1.3	36.5	4.4	72	27	38
$A4_{WB}$	5.61	1677.8	224.0	75.5 ± 1.5	28.3	5.2	73	33	46
$A3_{WB}$	6.35	2416.2	221.0	95.5 ± 1.9	21.3	6.6	83	47	58
$A2_{WB}$	6.84	3742.3	141.8	135.7 ± 2.7	10.1	9.5	89	73	82
$A1_{FB}$	7.68	5139.1	27.0	164.7 ± 3.2	1.5	11.7	100	100	100
ES_{WB}	2.29	203.5	461.6	22.8 ± 0.8	87.0	1.6			
GJ_{WB}	4.39	1870.9	635.3	106.5 ± 2.4	50.1	7.4			
$NJ1_{WB}$	0.88	167.7	101.2	48.4 ± 1.1	64.1	3.3			
$NS1_{WB}$	3.82	1054.1	207.9	69.8 ± 1.4	36.8	4.8	60	25	42
$NS2_{WB}$	4.72	1171.1	396.1	62.8 ± 1.3	50.0	4.3	75	27	38
$NS3_{WB}$	5.09	1293.6	426.9	64.3 ± 1.3	49.4	4.4	80	30	38
$NS4_{WB}$	5.15	1809.5	392.7	88.4 ± 1.9	39.1	6.1	81	42	53
$NS5_{WB}$	5.96	2235.9	419.8	94.2 ± 1.8	35.7	6.5	94	52	56
$NS6_{FB}$	6.33	4298.1	22.9	166.9 ± 3.6	1.5	11.9	100	100	100
$AS1_{WB}$	3.62	826.7	475.9	57.9 ± 1.2	63.0	4.0	53	19	36
$AS2_{WB}$	2.22	582.4	455.0	67.5 ± 2.0	69.9	4.6	32	13	42
$AS3_{WB}$	5.14	1209.9	388.8	60.7 ± 1.7	48.8	4.1	75	27	38
$AS4_{FB}$	6.84	4431.2	49.1	159.6 ± 4.6	3.2	11.3	100	100	100
9425_{WB}	2.56	796.8	23.8	78.5 ± 1.5	8.1	5.4	35	39	112
9424_{WB}	3.51	997.5	44.3	71.8 ± 1.5	11.6	5.0	48	49	102
9423_{WB}	3.64	775.9	204.7	54.1 ± 1.1	43.8	3.7	50	38	77
9422_{WB}	3.64	1018.8	57.7	70.7 ± 1.4	14.3	4.9	50	50	101
9421_{WB}	4.50	1270.1	87.1	71.3 ± 1.4	16.8	4.9	62	63	102
9420_{FB}	7.31	2030.4	105.7	70.2 ± 1.4	13.3	4.9	100	100	100
$NJ2\text{-}1_{WB}$	1.05	677.9	13.3	159.1 ± 3.1	5.5	11.3	48	53	111
$NJ2\text{-}2_{WB}$	2.27	1551.8	7.2	168.4 ± 3.2	1.4	12.0	103	122	118
$NJ2\text{-}3_{WB}$	1.08	846.7	7.0	192.1 ± 3.7	2.4	13.7	49	66	134
$NJ2\text{-}4_{WB}$	1.79	705.6	47.6	98.8 ± 1.9	16.6	6.9	81	55	69
$NJ2\text{-}5_{WB}$	1.27	649.9	17.5	127.6 ± 2.5	7.4	9.0	57	51	89
$NJ2\text{-}6_{FB}$	2.20	1274.4	42.8	143.2 ± 2.8	9.0	10.1	100	100	100
Standard sample (*recommended age* $= 18.5 \pm 0.6$ *Ma*)									
Bern21	8.68	616.7		18.2 ± 0.4	33.7				

[a] Sample types: WB, weathered biotite; FB, fresh biotite.
[b] Radiogenic ^{40}Ar.

biotite. In contrast, the slight decrease in the Rb content might be due to the very low Rb content of the weathering solution. The increasing Sr and decreasing Rb contents of the weathered biotites are likely related to the high Sr and low Rb contents of soluble plagioclase (Table 2). The $^{87}Sr/^{86}Sr$ ratio of the Sr introduced into the interlayer of vermiculite from the weathering solution is also probably similar to that of plagioclase. It is reasonable that the soluble plagioclase controls the isotopic and elemental composition of the weathering solution from following discussions. Petrographic observations showed that plagioclase is the most abundant (44 vol %) and reactive, whereas K-feldspar (5 vol %) and biotite (13 vol %) are minor components and much less reactive. In the upper part of the weathering profile, plagioclase dissolves actively forming kaolin minerals (Jeong and Kim, 2003), whereas oxidized

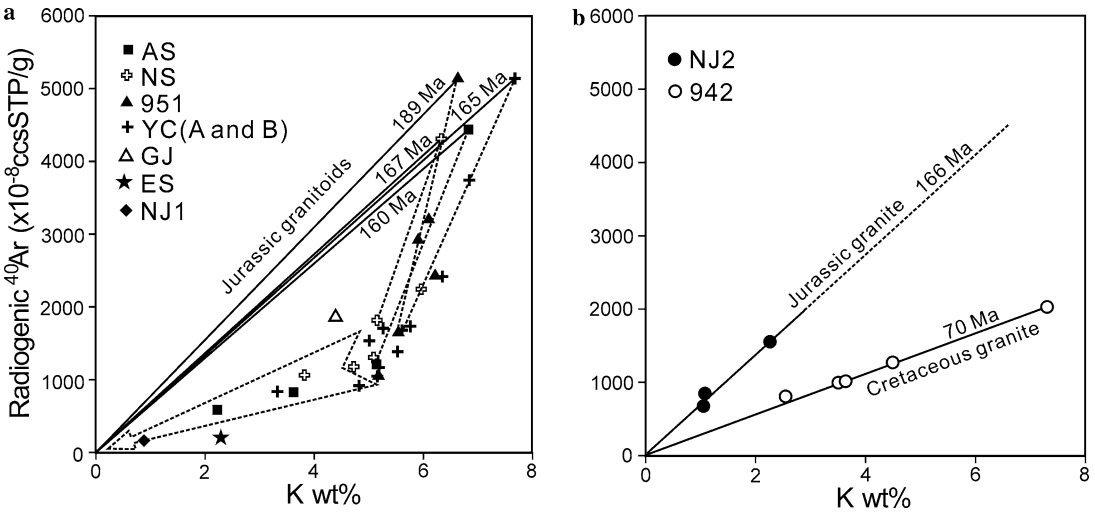

Fig. 7. K–Ar isotopic data plotted on K–^{40}Ar diagram. Solid lines connect origin with the data points of fresh biotites. Dashed lines and arrow in the diagram (a) indicate the early and later stages of the evolution of K–Ar isotopic systems. Three hydrobiotite data of the profile NJ2 in the diagram (b) are plotted with a regression line of which slope suggests the cooling age of bedrock as 166 Ma.

biotite is more resistant to dissolution after the early rapid chemical modification. Murphy et al. (1998) reported that oxidized biotite is the major primary mineral remaining in the tropical soil-saprolite weathering profile developed on granodiorite where plagioclase disappeared completely by dissolution. Sr isotopic data of weathered biotites are clustered near whole rock (or plagioclase) data in the Rb–Sr isochron diagram and approach toward the whole rock (or plagioclase) data with the progress of weathering (Fig. 6). These indicate that the Sr isotopic compositions of vermiculite interlayer of the weathered biotite are greatly influenced by the dissolution of plagioclase of relatively low $^{87}Rb/^{86}Sr$ and $^{87}Sr/^{86}Sr$ ratios though a very small contribution from biotite of high $^{87}Rb/^{86}Sr$ and $^{87}Sr/^{86}Sr$ ratios. Biotite may control the Sr isotopic compositions of the weathering solutions in recently deglaciated terrains where bedrocks undergo only an incipient weathering of active biotite oxidation and little plagioclase dissolution (Blum et al., 1994) or in the intensively weathered tropical profile lacking plagioclase (Murphy et al., 1998), but not in mature weathering profiles undergoing the active dissolution of plagioclase.

The ^{87}Sr content in the interlayer of oxidized biotite of the weathered biotite was calculated, assuming (1) the weathered biotite being composed of oxidized biotite and vermiculite, (2) the preservation of the $^{87}Sr/^{86}Sr$ ratio of fresh biotite in the interlayers of oxidized biotite, and (3) the $^{87}Sr/^{86}Sr$ ratio of vermiculite in the weathered biotite being equivalent to that of plagioclase. Four equations are established:

$$^{87}Sr_{WB} = {}^{87}Sr_B + {}^{87}Sr_V \quad (1)$$

$$^{86}Sr_{WB} = {}^{86}Sr_B + {}^{86}Sr_V \quad (2)$$

$$^{87}Sr_B/^{86}Sr_B = {}^{87}Sr_{FB}/^{86}Sr_{FB} = R_{FB} \quad (3)$$

$$^{87}Sr_V/^{86}Sr_V = {}^{87}Sr_P/^{86}Sr_P = R_P \quad (4)$$

where subscripts denote weathered biotite (WB), biotite in weathered biotite (B), vermiculite in weathered biotite (V), fresh biotite (FB), and plagioclase (P). From Eqs. (2)–(4), $^{87}Sr_V$ is expressed as

$$^{87}Sr_V = {}^{86}Sr_{WB}R_P - {}^{87}Sr_BR_P/R_{FB} \quad (5)$$

From Eqs. (1) and (5), $^{87}Sr_B$ (ppm) is calculated from the ^{87}Sr(ppm) and ^{86}Sr (ppm) of weathered biotite and the isotope weight ratios of fresh biotite (R_{FB}) and plagioclase (R_P) converted from atomic ratios.

$$^{87}Sr_B = R_{FB}(^{87}Sr_{WB} - {}^{86}Sr_{WB}R_P)/(R_{FB} - R_P) \quad (6)$$

The results are given in Table 2. The $^{87}Sr_B$ content decreases dramatically to 31% of the original content in sample A4, whereas Rb content decreases only slightly to 95% of the original content, implying a mass and preferential release of ^{87}Sr from the interlayers of oxidized biotite during the period of most active iron oxidation. Similarly, radiogenic ^{40}Ar content decreases to 33% of the original content in A4, whereas K content decreases to only 73% of the original content.

In the period of active iron oxidation from sample A1 to sample A4, this preferential release of ^{87}Sr and ^{40}Ar relative to respective Rb and K results in the progressive deviation of isotopic data from isochron and a significant reduction in the Rb–Sr and K–Ar ages during the early stages of weathering (Figs. 6 and 7). Cations including Fe and Mg in the octahedral sheet and K, Rb, and Sr in the interlayer are released to compensate excess positive charge induced by the oxidation of Fe^{2+} to Fe^{3+}. The preferential mobilization of radiogenic ^{87}Sr and ^{40}Ar is promoted by a local charge imbalance caused by the change in ionic charge and radius during radioactive decay. In the later stages of weathering, Rb–Sr and K–Ar data are plotted along straight lines toward the origin, indicating a proportional release of ^{87}Sr and ^{40}Ar relative to Rb and K and little changes in apparent ages.

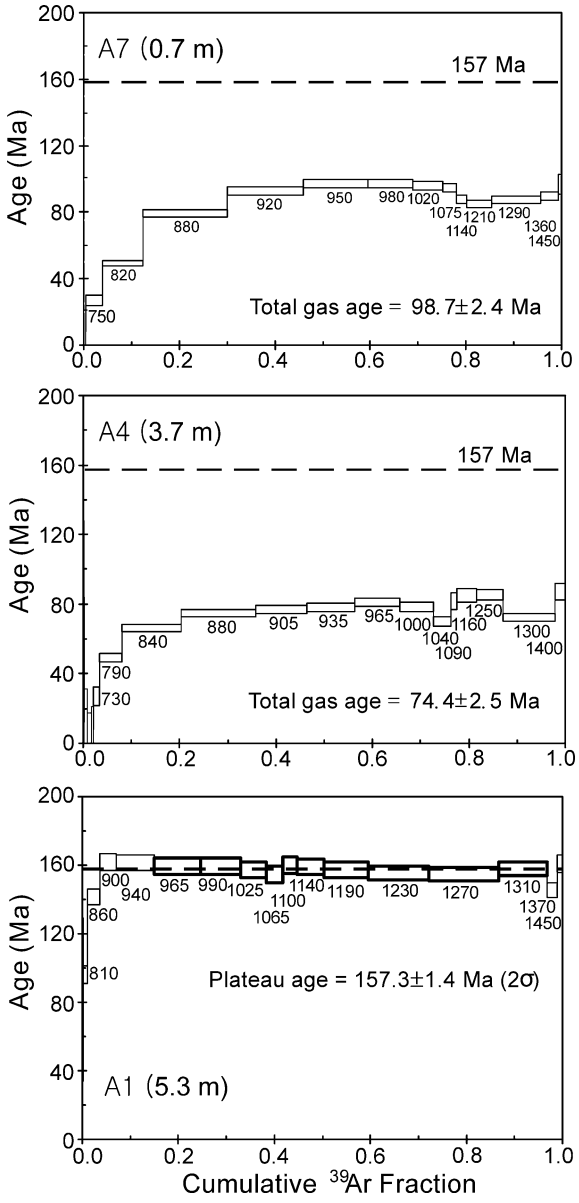

Fig. 8. Ar–Ar age spectra of fresh biotite (A1) and weathered biotites (A4 and A7) from the profile YC-A. Box heights in age spectrum represent 2σ uncertainties. Heating temperatures for Ar degassing in vacuo are given below the boxes.

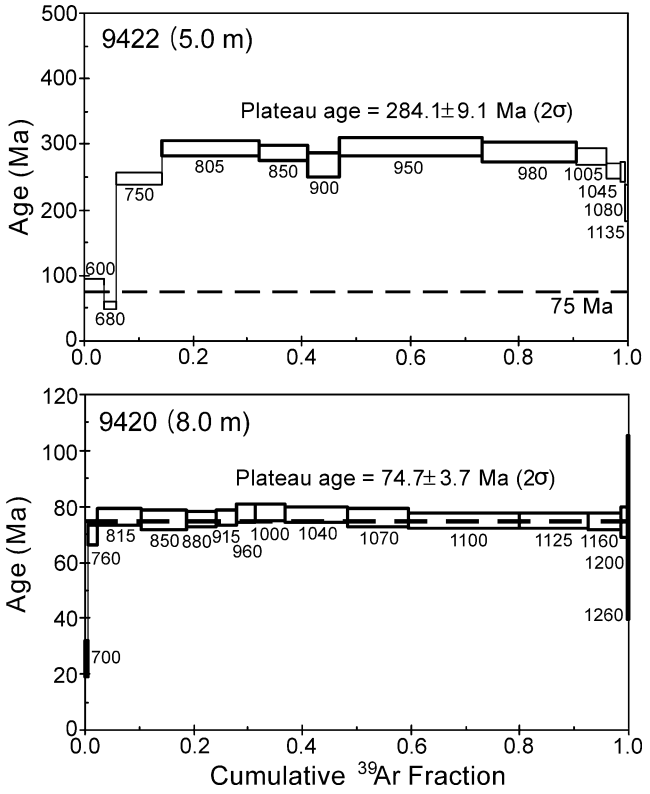

Fig. 9. Ar–Ar age spectra of fresh biotite (9420) and weathered biotite (9422) from the profile 942.

The loss of cations and isotopes by solid-state diffusion is indicated by both the mineralogical properties and ^{40}Ar–^{39}Ar age spectra. Since 10 Å basal spacing has been maintained during the iron oxidation period, it is inevitable that the loss of isotopes as well as Fe, Mg, and K occurred via diffusion through the non-expanded lattice of oxidizing biotite as discussed in Jeong and Kim (2003). The solid-state diffusion is also indicated by the shapes of the ^{40}Ar–^{39}Ar age spectra changing from the flat one (sample A1) to the curved one (samples A4 and A7). Because the interlayer water of vermiculite is completely degassed below 500 °C probably together with extraneous Ar in the interlayer of minor vermiculite, the apparent ages in the age spectra of samples A4 and A7 (Fig. 8) relate to the oxidized biotite. The total gas age of sample A4 is same as the conventional K–Ar age, indicating that crystals of oxidized biotite are sufficiently thick to trap ^{39}Ar during the neutron irradiation. However, in the age spectrum of sample A7, some escape of recoiling ^{39}Ar is indicated by the total gas age slightly higher than its conventional K–Ar age. This is reasonable because sample A7 is more weathered than sample A4, higher in vermiculite content, and more comminuted allowing the escape of recoiling ^{39}Ar. Nevertheless, the age spectrum of sample A7 was lowered far below that of fresh biotite (A1) with the loss of plateau. In both spectra, gradual increase in age toward higher-temperature degassing steps correlates well with the theoretical age spectra based on diffusion theory (Turner, 1968). It has been disputed whether ^{40}Ar–^{39}Ar age spectra of biotite from the vacuum stepwise extraction provide information on a natural gradient of ^{40}Ar formed by diffusion during the geological events such as contact metamorphism (Hanson et al., 1975; Ozima et al., 1979; Harrison et al., 1985; Gaber et al., 1988; Lo et al., 2000). Most studies concluded that initial ^{40}Ar distribution is lost by the significant structural, chemical, and morphological changes of biotite during the heating, resulting in the perturbed or flat age spectra regardless of the initial gradient (Hanson et al., 1975; Harrison et al., 1985; Gaber et al., 1988; Lo et al., 2000). However, the weathered biotites (A4 and A7) in this study were already oxidized in the weathering profile and underwent chemical and structural changes. Further changes in

vacuum stepwise-heating were likely less than generally thought in previous studies. Ozima et al. (1979) heated fresh biotite in air, and subsequently analyzed Ar isotopes by vacuum stepwise extraction. They obtained a stair-case increase of ages toward higher temperature steps similar to the age spectra of our oxidized biotites. Thus, the curved age spectra of the samples A4 and A7 reflect largely the original gradient of Ar concentration formed by the partial Ar loss via diffusion during the iron oxidation.

After the completion of oxidation, the oxidized biotite is subjected only to continued gradual vermiculitization and decomposition to kaolinite, in which both parent and daughter isotopes are indiscriminately removed from the interlayers. Extraneous ^{87}Sr was introduced into the interlayer of vermiculite, but the apparent Rb–Sr age was not affected by the simple mixing of the ambient weathering solution and biotite. Although extraneous ^{87}Sr was introduced into the minor vermiculitic interlayer even in the early period of active iron oxidation, the reduction in age results predominantly from the preferential release of radiogenic ^{87}Sr from the interlayer of oxidized biotite.

The Rb–Sr and K–Ar ages of biotites from saprolitic migmatite have been reported by Clauer (1981) and Clauer et al. (1982). Although they did not present detailed mineralogical data, a K_2O content of around 6% together with a low vermiculite content (Clauer et al., 1982) indicates that these weathered biotites must have been largely oxidized biotite. The behaviors of the Rb–Sr and K–Ar systems of these biotites with increasing degrees of weathering showed a concave curve below reference line (Clauer, 1981) which is quite similar to those observed in this study, but they didn't address the origin of such behaviors. The age reduction through the weathering profile can be interpreted as a two-stage process: the early preferential loss of ^{87}Sr and ^{40}Ar forced by iron oxidation and the later proportional loss after iron oxidation.

5.1.2. Hydrobiotite

Hydrobiotite was formed either directly from fresh biotite during the early active oxidation of iron (e.g. profile 942) or from the early-formed oxidized biotite (e.g. profile AS). In profile 942, the Sr contents of the weathered biotites are much lower than those of profile YC (Table 2), implying less introduction of extraneous Sr into the vermiculite interlayer of hydrobiotite, probably because the major interlayer cations are negligibly exchangeable hydroxy-Al cations (Table 1). Hydroxy-Al cations tend to be rich in the upper acidic part of weathering profiles (Banhisel and Bertsch, 1989; and references therein). They are increasingly fixed on the exchangeable sites of the vermiculite interlayer of hydrobiotites with the progress of weathering, resulting in the decrease of the sites for other exchangeable cations including Sr. Thus, with the progress of weathering from 9421 to 9425, Sr contents are generally lowered (Table 2), and $^{87}Sr/^{86}Sr$ and $^{87}Rb/^{86}Sr$ ratios approach those of fresh biotite on the isochron (Fig. 6).

^{87}Sr content in the biotite interlayer was calculated according to the method as discussed above. Since plagioclase (31 vol %) is richer and far more reactive than K-feldspar (31 vol %) and biotite (5 vol %) in granite bedrock, the isotopic compositions of weathering solutions are largely controlled by the dissolution of plagioclase. Both ^{87}Sr and Rb contents decrease in proportion rapidly to 50% of their original levels (Table 2), which is consistent with the formation of hydrobiotite, a 1:1 regularly interstratified biotite-vermiculite. The formation of hydrobiotite in sample 9421 during the period of active iron oxidation indicates that iron oxidation forced the early mass and proportional release of interlayer cations and isotopes. Both ^{87}Sr and Rb contents decrease further to 36% of the original contents in sample 9425 in the latest stage of weathering by the kaolinitization. Both ^{40}Ar and K also behaved like ^{87}Sr and Rb, respectively. Despite significant structural and chemical transformations, all the daughter isotopes ^{87}Sr and ^{40}Ar must have remained in the alternating biotite interlayers because any removal of interlayer cations via diffusion from the non-expanded biotite interlayer would have resulted in their preferential removal of ^{87}Sr and ^{40}Ar as shown in the case of oxidized biotite.

In the ^{40}Ar–^{39}Ar age spectrum of sample 9422, ^{39}Ar recoiled from the biotite interlayer might have escaped along the alternating vermiculite interlayer, greatly raising the apparent age relative to that of fresh biotite in sample 9420. Nevertheless, the plateau in the age spectrum of sample 9422 indicates that there was little preferential loss of Ar via diffusion during the formation of hydrobiotite. As discussed in previous section, the plateau of the hydrobiotite 9422 is likely to reflect an initial distribution of Ar but not an artifact during the vacuum stepwise heating.

The proportional release of parent and daughter isotopes from vermiculitizing interlayer and their complete preservation in the alternating biotite interlayer result in the complete preservation of the original Rb–Sr and K–Ar isotopic ages. Extraneous Sr in the weathering solution originated predominantly from actively dissolving plagioclase was introduced into the vermiculite interlayer of hydrobiotite, but did not affect the Rb–Sr ages. The location of data on the isochron was determined by the simple isotopic mixing between hydrobiotite and the weathering solution largely controlled by plagioclase dissolution. The decomposition of hydrobiotite to kaolinite, followed by a proportional release of radiogenic elements, did not change the original ages.

In sample 9423, a preferential leaching of ^{87}Sr over Rb and ^{40}Ar over K is evident, implying the presence of oxidized biotite. Because Fe was almost completely oxidized in sample 9423, $B_{82}V_{18}$, the major component in sample 9423, consists mostly of oxidized biotite (82%) from which daughter isotopes ^{87}Sr and ^{40}Ar were preferentially leached. The abnormal behavior of sample 9423 might reflect weathering conditions at that position different from those at the other sample locations; for instance, the presence of specific fracture patterns as a conduit of weathering

solution or the difference in mineralogical and chemical characteristics of the fresh biotite.

In profiles NS and AS, hydrobiotite developed from early-formed oxidized biotite. The radiogenic ^{87}Sr and ^{40}Ar of the oxidized biotite were preserved in the alternating interlayers, resulting in the preservation of the apparent age of the oxidized biotite. The preservation of isotopic age in the transformation of oxidized biotite to hydrobiotite was similar to that in the transformation of fresh biotite to hydrobiotite in profile 942.

5.1.3. Relation between Rb–Sr and K–Ar systems

In Fig. 10, the isotopic ages of oxidized biotites (profiles YC and AS) are compared with those of hydrobiotites (profile 942). The Rb–Sr ages are systematically lower than the K–Ar ages as reported in Clauer et al. (1982). In both profiles 942 and YC, the daughter isotopes ^{87}Sr and ^{40}Ar in the interlayer of biotites decrease proportionally to each other throughout the profiles (Fig. 11a). In profile 942, the parent elements Rb and K decrease in proportion (Fig. 11b). However, in profile YC, K decreases more rapidly than Rb during the period of active iron oxidation from fresh biotite to oxidized biotite (Fig. 11b). From A1 to A4, K content decreases by 27%, whereas the Rb content decreases by only 5%. After the nearly complete oxidation of iron, the Rb content decreases by 38% from A4 to B4, concomitant with a decrease in the K contents by 30%. The preferential removal of K relative to Rb might be related to smaller ionic radius of $K^+$and its less selectivity on a mineral surface (Sposito, 1989).

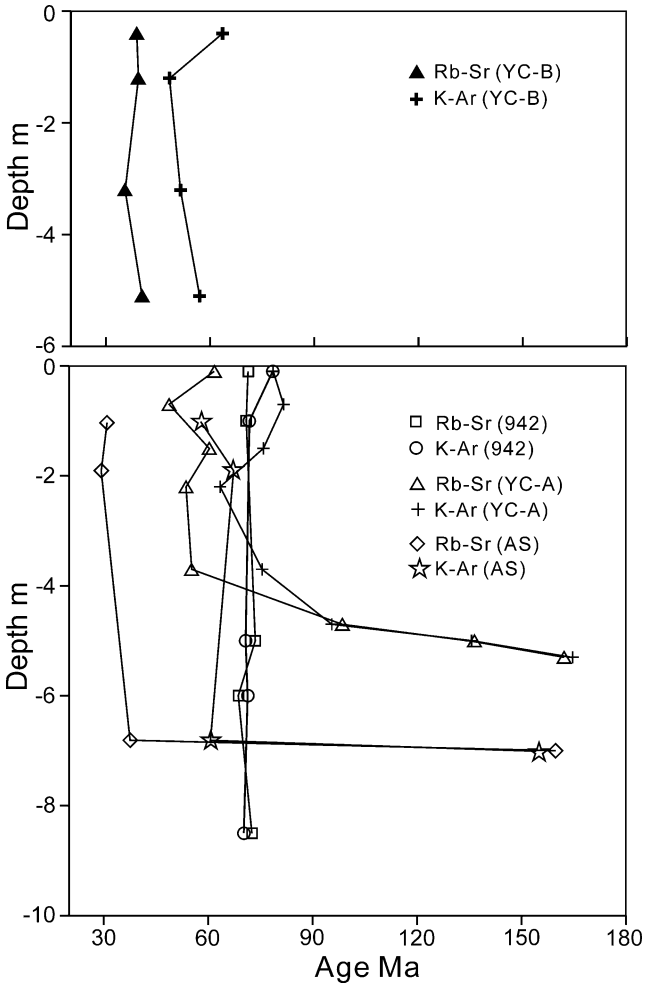

Fig. 10. Rb–Sr and K–Ar isotopic ages of four profiles plotted on the diagrams of age vs. depth.

5.2. Implications

5.2.1. Isotopic dating

As shown above, the hydrobiotite that develops during early active iron oxidation is useful for the Rb–Sr and K–Ar isotopic dating of lithological units subjected to weathering. However, in many cases, biotite loses its original isotopic age during its early transformation into oxidized biotite. Hydrobiotite that has transformed from oxidized biotite is not useful for dating bedrock. Whole-rock dating can be tried to date the weathered equivalent of bedrock lacking biotite, because the preferential release of radiogenic elements is not significant during the weathering of the other common K-minerals. K-feldspars dissolve in a stoichiometric pattern (Blum and Stillings, 1995). Muscovite is more highly resistant to weathering than biotite (Rausell-Colom et al., 1965), and tends to decompose to kaolinite without the formation of vermiculite (Jeong, 1998). Worden and Compston (1973) showed that the whole-rock age of Archean granite was surprisingly well preserved, even in completely weathered samples of laterite profiles. Their petrographic descriptions of fresh and weathered samples did not report any biotite or its weathering products, so these whole-rock ages were possibly preserved by the absence of biotite.

There have been several attempts to use biotite as a proxy for sediment provenance (Michell and Taka, 1984; Mitchell et al., 1988; Renne et al., 1990). Our study revealed that the weathering pathway of biotite and their apparent ages vary little from site to site within a stock or small batholith of several tens of kilometers in size, but often vary significantly from stock to stock or from batholith to batholith. Biotites in the sediments derived from soil and saprolite in the source area were mostly oxidized biotite or hydrobiotite because iron oxidation occurs very rapidly in the lower parts of the weathering profiles. Thus, the mineralogy and apparent age of weathered biotite can be a useful tool for tracing the source areas of biotite-bearing sediments.

5.2.2. Sr isotopic compositions of hydrological regimes

The Sr isotopic compositions of hydrological regimes depend on the ages and Rb/Sr ratios of rocks and on mineral solubilities. Biotite is a major reservoir of radiogenic ^{87}Sr in igneous and metamorphic rocks. Faure (1986) expected that Sr is lost more readily from rocks than Rb, mainly by plagioclase dissolution, resulting in the enrichment of ^{87}Sr in

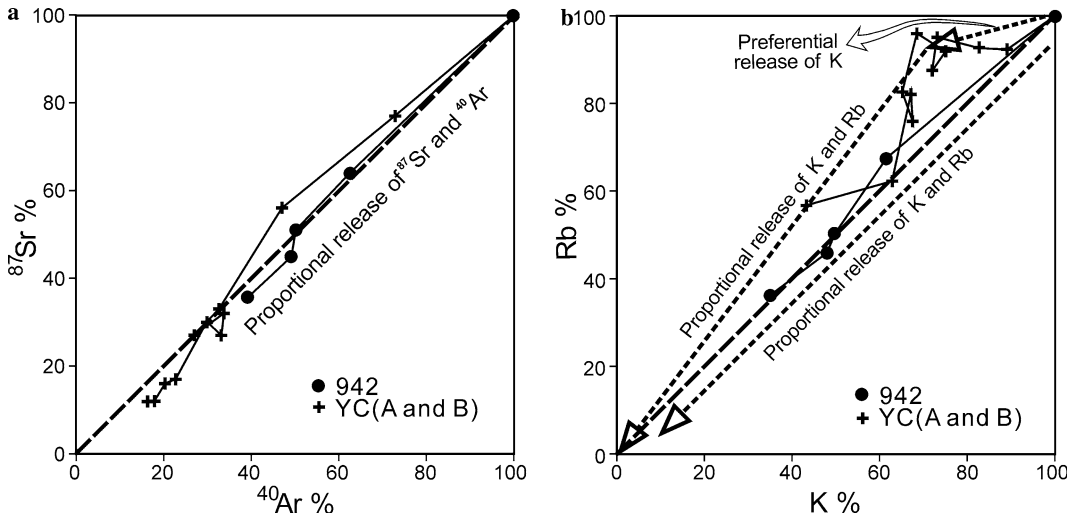

Fig. 11. Release patterns of daughter isotopes ^{87}Sr and ^{40}Ar and their parent elements Rb and K. (a) Proportional release of daughter isotopes in both profiles. (b) Proportional release of parent elements in profile 942, but early preferential release of K over Rb and later proportional release of K and Rb in profile YC (A and B).

weathered rocks. However, as shown in our study, biotite released 50–60% of its ^{87}Sr in the very early stages of weathering. In the weathering profile of K-feldspar-poor granodiorite (profile YC), the whole-rock ^{87}Sr/^{86}Sr ratio decreased predominantly with the preferential release of ^{87}Sr from oxidized biotite. In profile 942, developed on K-feldspar-rich (31 vol%) granite, the increase in the whole-rock ^{87}Sr/^{86}Sr ratio was not great. The early preferential depletion of radiogenic ^{87}Sr from weathering biotite particularly in the environments undergoing incipient weathering causes to increase ^{87}Sr/^{86}Sr ratios in the ambient groundwaters and stream waters (Blum et al., 1994), and in the exchange pool in the soil (Blum and Erel, 1997). Based on dissolution experiments with granitoids, Erel et al. (2004) suggested that the weathering flux in younger soils is controlled by elemental release from the interlayer of biotite in the early stage of weathering. Taylor et al. (2000) showed that the release of radiogenic ^{87}Sr results in an increase in the apparent Rb–Sr ages, which contradicts to the natural trend of decreasing apparent ages.

Our study shows that two stages of biotite weathering should be considered in any model of the Sr isotopic composition of the stream water that drains the watershed on biotite-bearing bedrock. In a deep saprolitic weathering profile, there is a gradient in the degree of weathering and permeability that extends from the old upper soil horizon, which lacks plagioclase, to the young lowermost part undergoing incipient weathering. In the upper highly weathered part, the ionic and Sr isotopic contribution from the profile is governed by slow stoichiometric weathering or interlayer hydration, whereas in the very slightly weathered lower part, it is governed by the rapid oxidative weathering of biotite with a concomitant mass release of ^{87}Sr. The cationic and Sr isotopic compositions of the hydrological regime will be a combination of the contributions from throughout the weathering profiles.

6. Conclusions

The responses of biotite isotopic systems to weathering are dependent upon the weathering processes, including iron oxidation, structural transformation, and decomposition. Early iron oxidation forces a mass release of daughter isotopes ^{87}Sr and ^{40}Ar. Their preferential removal relative to that of Rb and K via solid-state diffusion during the transformation to oxidized biotite results in the reduction of the original isotopic age, whereas their proportional removal during the transformation to hydrobiotite results in the preservation of the original age. In the upper part of the profile, ^{87}Sr, Rb, ^{40}Ar, and K are gradually and

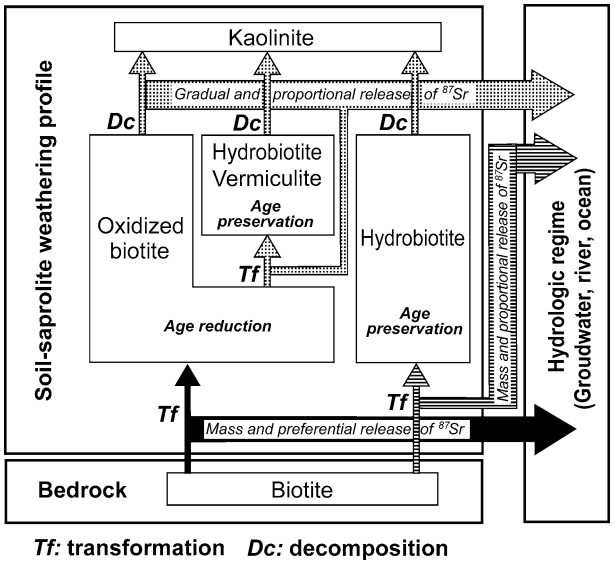

Fig. 12. Models of mineralogical pathways of biotite weathering and corresponding behaviors of Rb–Sr and K–Ar isotopic systems with release patterns of strontium isotopes into hydrologic regimes. ^{87}Sr is released proportionally or preferentially relative to ^{87}Rb.

proportionally released with no further change in the isotopic age. General models of biotite weathering and the behaviors of isotopic systems are summarized in Fig. 12. Regional variations in the isotopic systems regulated by weathering processes should be considered when dating biotite-bearing rocks in weathering environments, modeling the input of Sr isotopes to hydrological cycles, and tracking sediment provenance.

Acknowledgments

The manuscript was improved by Albert Galy and two anonymous reviewers. We thank Y.-J. Jeong for Sr isotope analysis. This work was supported by the Korea Research Foundation (Project No. KRF–2000–DP0433).

Associate editor: S. Krishnaswami

References

Banhisel, R.I., Bertsch, P.M., 1989. Chlorites and hydroxy-interlayered vermiculite and smectite. In: Dixon, J.B., Weed, S.B. (Eds.), *Minerals in Soil Environment*. Soil Science Society of America, Madison, pp. 729–788.

Blum, A.E., Stillings, L.L., 1995. Feldspar dissolution kinetics. In: White, A.F., Brantley, S.L. (Eds.), *Chemical Weathering Rates of Silicate Minerals. Reviews in Mineralogy 31*. Mineralogical Society of America, Washington, D.C., pp. 291–351.

Blum, J.D., Erel, Y., Brown, K., 1994. $^{87}Sr/^{86}Sr$ ratios of Sierra Nevada stream waters: implication for relative mineral weathering rates. *Geochim. Cosmochim. Acta* **58**, 5019–5025.

Blum, J.D., Erel, Y., 1997. Rb-Sr isotope systematics of a granitic soil chronosequences: The importance of biotite weathering. *Geochim. Cosmochim. Acta* **61**, 3193–3204.

Brass, G.W., 1976. The variation of the marine $^{87}Sr/^{86}Sr$ ratio during Phanerozoic time: interpretation using a flux model. *Geochim. Cosmochim. Acta* **40**, 721–730.

Bullen, T., White, A., Blum, A., Harden, J., Schulz, M., 1997. Chemical weathering of a soil chronosequence on granitoid alluvium: II. Mineralogic and isotopic constraints on the behaviour of strontium. *Geochim. Cosmochim. Acta* **61**, 291–306.

Cheong, C.-S., Kwon, S.T., Kim, J., Chang, B.U., 1998. Geochemical and isotopic study of the Onjeongri granite in the northern Gyeongsang basin, Korea: Comparison with Cretaceous to Tertiary granitic rocks in the other part of the Gyeongsang basin and the inner zone of Southwest Japan. *J. Petrol. Soc. Korea* **7**, 77–97.

Clauer, N., 1981. Strontium and argon isotopes in naturally weathered biotites, muscovites and feldspars. *Chem. Geol.* **31**, 325–334.

Clauer, N., O'Neil, J.R., Bonnot-Courtois, C., 1982. The effect of natural weathering on the chemical and isotopic compositions of biotites. *Geochim. Cosmochim. Acta* **46**, 1755–1762.

Edmond, J.M., 1992. Himalayan tectonics, weathering processes, and the strontium isotope record in marine limestones. *Science* **258**, 1594–1597.

Erel, Y., Blum, J.D., Roueff, E., Ganor, J., 2004. Lead and strontium isotopes as monitors of experimental granitoid dissolution. *Geochim. Cosmochim. Acta* **68**, 4649–4663.

Faure, G., 1986. Isotope Geology of Strontium in Sedimentary Rocks. In: *Principles of Isotope Geology*. John Wiley, New York, pp. 183–199.

Fordham, A.W., 1990. Formation of trioctahedral illite from biotite in a soil profile over granite gneiss. *Clays Clay Miner.* **38**, 187–195.

Gaber, L.J., Foland, K.A., Corbató, C.E., 1988. On the significance of argon release from biotite and amphibole during $^{40}Ar/^{39}Ar$ vacuum heating. *Geochim. Cosmochim. Acta* **52**, 2457–2465.

Goldich, S.S., Gast, P.W., 1966. Effects of weathering on the Rb–Sr and K–Ar ages of biotite from the Morton Gneiss, Minnesota. *Earth Planet. Sci. Lett.* **1**, 372–375.

Hanson, G.N., Simmons, K.R., Bence, A.E., 1975. $^{40}Ar/^{39}Ar$ spectrum ages for biotite, hornblende and muscovite in a contact of metamorphic zone. *Geochim. Cosmochim. Acta* **39**, 1269–1277.

Harris, W.G., Zelazny, J.C., Baker, J.C., Martens, D.C., 1985. Biotite kaolinitization in Virginia Piedmont soils: I. Extent, profile trends, and grain morphological effects. *Soil Sci. Soc. Am. J.* **49**, 1290–1297.

Harrison, T.M., Duncan, I., McDougall, I., 1985. Diffusion of ^{40}Ar in biotite: temperature, pressure and compositional effects. *Geochim. Cosmochim. Acta* **49**, 2461–2468.

Jeong, G.Y., 1998. Vermicular kaolinite epitactic on primary phyllosilicates in the weathering profiles of anorthosite. *Clays Clay Miner.* **46**, 509–520.

Jeong, G.Y., Kim, H.B., 2003. Mineralogy, chemistry, and formation of oxidized biotite in the weathering profile of granitic rocks. *Am. Miner.* **88**, 352–364.

Krishnaswami, S., Trivedi, J.R., Sarin, M.M., Ramesh, R., Sharma, K.K., 1992. Strontium isotopes and rubidium in the Ganga–Brahmaputra river system: weathering in the Himalaya, fluxes to the Bay of Bengal and contributions to the evolution of oceanic $^{87}Sr/^{86}Sr$. *Earth Planet. Sci. Lett.* **109**, 243–253.

Kulp, J.L., Engels, J., 1963. Discordance in K–Ar and Rb isotopic ages. In: Radioactive dating. International Atomic Energy Agency, Vienna, pp. 219–238.

Lo, C.-H., Lee, J.K.W., Onstott, T.C., 2000. Argon release mechanisms of biotite in vacuo and the role of short-circuit diffusion and recoil. *Chem. Geol.* **165**, 135–166.

Ludwig, K.R. (2001) Users Manual for Isoplot/Ex Rev. 2.49, A Geochronological Toolkit for Microsoft Excel. Berkeley Geochronology Center Special Publication No. 1a. Berkeley, CA, USA.

McDougall, I., Harrison, T.M., 1999. *Geochronology and Thermochronology by the $^{40}Ar/^{39}Ar$ Method*. Oxford University Press, New York.

Michell, J.G., Taka, A.S., 1984. Potassium and argon loss patterns in weathered micas: implications for detrital mineral studies, with particular reference to the Triassic palaeogeography of the British Isles. *Sed. Geol.* **39**, 27–52.

Mitchell, J.G., Penven, M., Ineson, P.R., Miller, J.A., 1988. Radiogenic argon and major-element loss from biotite during natural weathering: a geochemical approach to the interpretation of potassium-argon ages of detrital biotite. *Chem. Geol. (Isot. Geosci. Sec.)* **72**, 111–126.

Murakami, T., Utsunomiya, S., Yokoyama, T., Kasama, T., 2003. Biotite dissolution processes and mechanisms in the laboratory and in nature: early stage weathering environment and vermiculitization. *Am. Miner.* **88**, 377–386.

Murphy, S.F., Brantley, S.L., Blum, A.E., White, A.F., Dong, H., 1998. Chemical weathering in a tropical watershed, Luquillo Mountains, Puerto Rico: II. Rate and mechanism of biotite weathering. *Geochim. Cosmochim. Acta* **62**, 227–243.

Ozima, M., Kaneoka, I., Yanagisawa, M., 1979. Temperature and pressure effects on ^{40}Ar–^{39}Ar systematics. *Earth Planet. Sci. Lett.* **42**, 463–472.

Palmer, M.R., Edmond, J.M., 1989. The strontium isotope budget of the modern ocean. *Earth Planet. Sci. Lett.* **92**, 11–26.

Rausell-Colom, J.A., Sweatman, T.R., Wells, C.B., Norrish, K., 1965. Studies in the artificial weathering of mica. In: Hallsworth, E.G., Crawford, D.V. (Eds.), *Experimental Pedology*. Butterworths, London, pp. 40–72.

Renne, P.R., Becker, T.A., Swapp, S.M., 1990. $^{40}Ar/^{39}Ar$ laser-probe dating of detrital micas from the Montgomery Creek Formation, northern California: clues to provenance, tectonics, and weathering processes. *Geology* **18**, 563–566.

Renne, P.R., Swisher, C.C., Deino, A.L., Karner, D., Owens, T.L., DePaolo, D.J., 1998. Intercalibartion of standards, absolute ages and uncertainties in $^{40}Ar/^{39}Ar$ dating. *Chem. Geol.* **145**, 117–152.

Reynolds, R.C. Jr., 1985. NEWMOD A Computer Program for the Calculation of One-Dimensional Diffraction Patterns of Mixed-Lay-

ered Clays. R.C. Reynolds Jr., 8 Brook Dr., Hanover, New Hampshire.

Richter, F.M., Rowley, D.B., DePaolo, D.J., 1992. Sr isotope evolution of seawater: the role of tectonics. *Earth Planet. Sci. Lett.* **109**, 11–23.

Sagong, H., Kwon, S.T., Ree, J.H., 2005. Mesozoic episodic magmatism in South Korea and its tectonic implication. *Tectonics* **24**, TC5002. doi:10.1029/2004TC001720.

Scott, A.D., Amonette, J., 1988. Role of iron in mica weathering. In: Stucki, J.W., Schwertmann, U. (Eds.), *Iron in Soils and Clay Minerals*. Springer, Dordrecht, Holland, pp. 537–625.

Sposito, G., 1989. *The Chemistry of Soils*. Oxford University Press, New York.

Taylor, A., Blum, J.D., Lasaga, A., MacInnes, I.N., 2000. Kinetics of dissolution and Sr release during biotite and phlogopite weathering. *Geochim. Cosmochim. Acta* **64**, 1191–1208.

Turner, G., 1968. The distribution of potassium and argon in chondrites. In: Ahrens, L.H. (Ed.), *Origin and Distribution of the Elements*. Pergamon, London, pp. 387–398.

Worden, J.M., Compston, W., 1973. A Rb–Sr isotopic study of weathering in the Mertondale granite, Western Australia. *Geochim. Cosmochim. Acta* **37**, 2567–2576.

Zartman, R.E., 1964. A geochronologic study of the Lone Grove Pluton from the Llano Uplift, Texas. *J. Petrol.* **5**, 359–408.